Front. Struct. Civ. Eng. 2022, 16(6): 667–684
https://doi.org/10.1007/s11709-022-0822-4

RESEARCH ARTICLE

A hierarchical system to predict behavior of soil and cantilever sheet wall by data-driven models

Nang Duc BUI[a], Hieu Chi PHAN[b*], Tiep Duc PHAM[a], Ashutosh Sutra DHAR[b]

[a] *Institute of Techniques for Special Engineering, Le Quy Don Technical University, Hanoi 100000, Vietnam*
[b] *Faculty of Engineering and Applied Science, Memorial University of Newfoundland, St. John's, NL A1B 3X5, Canada*
[*] *Corresponding author. E-mail: hcp082@mun.ca*

ABSTRACT The study proposes a framework combining machine learning (ML) models into a logical hierarchical system which evaluates the stability of the sheet wall before other predictions. The study uses the hardening soil (HS) model to develop a 200-sample finite element analysis (FEA) database, to develop the ML models. Consequently, a system containing three trained ML models is proposed to first predict the stability status (random forest classification, RFC) followed by 1) the cantilever top horizontal displacement of sheet wall (artificial neural network regression models, RANN1) and 2) vertical settlement of soil (RANN2). The uncertainty of this data-driven system is partially investigated by developing 1000 RFC models, based on the application of random sampling technique in the data splitting process. Investigation on the distribution of the evaluation metrics reveals negative skewed data toward the 1.0000 value. This implies a high performance of RFC on the database with medians of accuracy, precision, and recall, on test set are 1.0000, 1.0000, and 0.92857, respectively. The regression ANN models have coefficient of determinations on test set, as high as 0.9521 for RANN1, and 0.9988 for RANN2, respectively. The parametric study for these regressions is also provided to evaluate the relative insight influence of inputs to output.

KEYWORDS finite element analysis, cantilever sheet wall, machine learning, artificial neural network, random forest

1 Introduction

In urban areas, construction activities are commonly restricted due to the high density of adjacent buildings. This leads to the requirement of retaining walls to reduce the excavation area impact on movement. A cantilever sheet wall is a regular retaining structure for the shallow excavation, and the stability of this structure relies on the balance of the active, and passive, soil pressures. The cause of failure primarily comes from the failure of maintaining this balance rather than exceeding the allowable stress in the wall. This failure may lead to the collapse of the adjacent building or buildings, and thus, accurately predicting the failure or stability of the cantilever is desired for not only the construction works itself, but also the surrounding environment. The horizontal displacement at the top of the cantilever sheet wall (Δ), can affect the working space within the excavation and be the alarm of the wall collapse, is a very complicated prediction because of its combinations of rotation due to imperfect supports and deflection of the wall. The ground movement, $y(x)$, due to the excavation, is a potential failure thread to the adjacent building or their piles. Consequently, the soil settlement adjacent to a sheet wall is also a variable [1–5] of interest.

The finite element analysis (FEA), is a common approach to solve geotechnical problems and is commonly applied for the designing purpose as in Ref. [6]. However, FEA sometimes faces difficulty with solving the partial differential equations for complicated problems, and only yields to the prediction for a particular case without extracting the non-relationship of the input variables. It provides an approximation model [8]. Practical approaches to eliminate these drawbacks are commonly relegated to a machine learning (ML) technique: 1) applying ML techniques to solve the partial differential equations as in Refs. [9,10], and 2) using FEA to generate the database for the ML models [10–13].

Article history: Received Aug 15, 2021; Accepted Jan 7, 2022

The combination of FEA for developing the database, and predicting the output, with ML models as summarized in Ref. [15], has been conducted not only for structural analyses [15–18] but also for a variety of geotechnical problems. Examples are modeling soil behaviour [19–22], predicting pile capacity [23–25], site characterization [26–28], liquefaction [29–31], slope stability [32–34], and landslide assessment [35–37]. Within these studies, research on the retaining structures is a critical part [1,13,38–41]. In Ref. [38], the conventional reliability approach (i.e., First Order Reliability Method and Monte Carlo Simulation) is integrated with artificial neural network (ANN) for reliability and risk evaluation of deep excavations. In Ref. [49], the displacement of a braced retaining wall in clay soil is predicted with the combination of ANN and FEA. In Ref. [1], the prediction on the additional deformation of the soil due to the nearby underground excavation and the parameter study, is implemented. In Ref. [13], records from construction site are used as the database to develop the ANN model for approximation of diaphragm wall deflection. The same concerns are on the retaining wall of deep excavation, in Ref. [40], the adaptive Broyden-Fletcher-Goldfarb-Shanno algorithm, and the neural network, are combined to estimate the state-based wall deflection and maximum location of each value. In Refs. [41–43], the surface settlement due to a deep foundation construction process has been predicted by random forest (RF) and ANN.

In contradiction, the ML approaches have several flaws such as the uncertainty in finding the "best" hyperparameters for the model. This leads to frequent use of a trial and error process and grid searching, or another optimization process is required in Refs. [7,44]. Furthermore, researcher who applied data-driven models for the geotechnical problems commonly focused on the single predicting task rather than proposing a system predicting various outputs regarding to the fact that the calculation be terminated with error. There is an absence of an initial classification model to observe soil-structure system failure possibility, and a shortage within current studies. Most studies have concentrated on the regression model where the variables of interest are continuous. Zhang et al. [45] summarized 92 studies with a soft computing approach, and the classification problem is rarely seen in this list, except for some on rock burst problems. Analogously, the review paper of Moayedi et al. [14], has shown this shortage.

In this study, a variable of interest, which is a binary variable, attached at the initial step of the predicting system, can be linguistically interpreted as "failure" or "not failure". It is obvious that this category and other continuous variables, such as quantities of ground settlement, have a hierarchical order in the prediction process. The proposed system is a simplified network, which contains a sequence of a classification model, the random forest classification (RFC), and is chosen to predict the stability status of the cantilever sheet wall. Two other regression ANN models (RANN1 and RANN2), predicting the vertical settlement of the adjacent ground surface, and the horizontal displacement, are conducted separately. The uncertainty of the ML model is observed by a random sampling technique in the train/test data splitting process for the classification problem. A set of 1000 RFC models is obtained and selection, from this set, is implemented to choose the "best" model for predicting status of the soil-structure system. The configuration selection process for the ANN model is conventionally carried out based on the trial and error approach, and not provided in the context for the sake of simplicity. The parametric study is implemented for the regression models, and the practical application of the proposed data-driven based hierarchical system is illustrated.

2 Methodology

2.1 Simulating behaviour of cantilever sheet wall with finite element analysis

Geometric variables of the sheet wall structure provided in Fig. 1(a), includes the depth of excavation H, length of the sheet wall L, and depth of the ground water table H_w. The addition of construction loads, such as vehicle load, or temporary weight load, are also modelled as a uniform load q, with the corresponding width of B along the x-axis. In some simulations, this load is not applied to widen the possible cases of the database. Material property (i.e., modulus of elasticity of steel, E) is combined with cross-section property of sheet wall (the moment of inertia, I) by using EI as an input variable. Cantilever sheet wall, and soil are modelled in Plaxis, as a 2D beam, and triangular two-dimensional deformation element, respectively. The meshing system includes the global mesh which is relatively coarse, and the mesh surrounds the sheet wall which is finer (Fig. 1(b)).

For geotechnical engineering, it is critical to choose a proper model to simulate the soil behaviour. Hardening soil (HS), is the model chosen in this paper, has an advantage in accounting for the effect of stress to the stiffness of soil [46–48]. This characteristic is appropriate, especially for the excavating process with different phases. The HS is a hyperbolically elastic-plastic model which additionally uses the secant stiffness in standard drain triaxial test E_{50ref}, tangent stiffness for primary oedometer loading E_{oed}, and unloading/reloading stiffness E_{urref}, to describe the stress-depend stiffness. It is commonly assumed that $E_{50ref} = E_{oed}$, and $E_{urref} = 3 \times E_{50ref}$ [46], and it is sufficient to account only E_{oed}, to the ML models because of these relationships.

Along with E_{oed}, the friction angle φ, cohesion c, saturated weight γ_{sat}, and unsaturated weight γ_{unsat}, are the 5 primary properties of soil required for the analysis process. Detail of the ranges of soil properties is to be provided in Section 3. These soil properties are collected by the author's team from various construction sites in Vietnam covering both cohesive and non-cohesive soils. Other additional properties of the soil such as natural water content, natural voids ratio, grain size distribution, degree of saturation, etc., are not always available in the collected data. These properties are not used to develop the prediction models, and can be found from their relationship with the 5 primary properties or reasonably assumed for the FEA. Soil with zero cohesion, will have this value set as 1 to ensure numerical stability in the computing process. Only homogeneous soil types, without stratification, and their long-term behaviour, are considered in this paper.

Each simulation starts with the first phase when the wall is inserted. The digging process is consequently taken place with 5 phases corresponding to soil layers, which equal to 1:5 of H (Fig. 1(b)). Response of the structure, such as wall and soil displacement found in each phase, is used as the input for the succeeding phase.

To avoid the collapse of Plaxis from other non-failure causes, the sheet wall structure is considered to be in failure if the "soil body collapses" announcement is applied. This equates to that the current stiffness parameter, *CSP*, is less than 0.015 (as default). *CSP* is a parameter to measure the amount of plasticity occurring in the calculation, where the near zero value of *CSP* indicates failure of the model [49]. The "soil body collapses" error, thus implies the ultimate limit state of the soil is exceeded and will be used as the collapse criterion. Additionally, if the horizontal displacement at the top of sheet wall is significantly large, it is a warning of exceeding the deformation limit (i.e., serviceability limit state). In general, a sheet wall applied for an excavation will be considered as failure if it collapses or exceeds a threshold for Δ. Since there is no strict rule for this threshold, it is practically chosen at 200 mm based on expert opinions.

The status of the structure and horizontal displacement at the top of the sheet wall can be written as the function

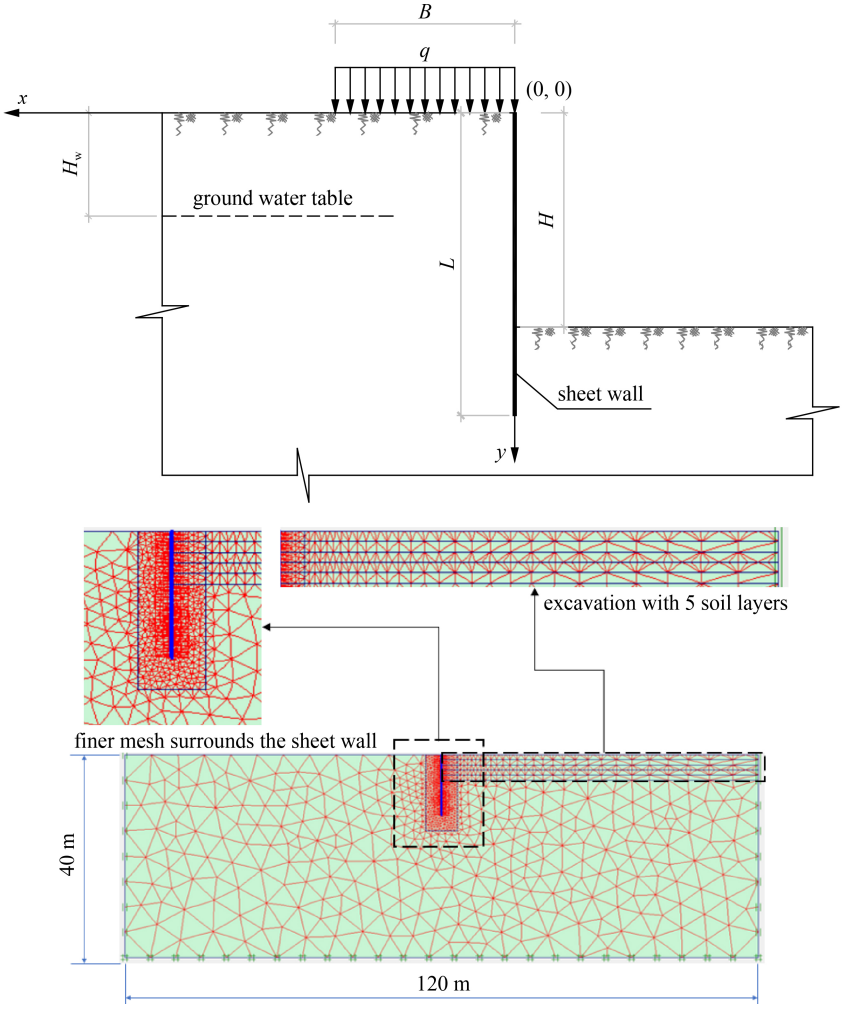

Fig. 1 Layout of the cantilever sheet wall with geometric input variables and the mesh grids and phase-based soil layers.

of input variables previously discussed:

$$Status = f(L, EI, H, H_w, B, q, E_{oed}, \gamma_{sat}, \gamma_{unsat}, \phi, c), \quad (1)$$

$$\Delta = f(L, EI, H, H_w, B, q, E_{oed}, \gamma_{sat}, \gamma_{unsat}, \phi, c). \quad (2)$$

Database for the vertical settlement of the ground is based on simulations but distinct from database for the status and Δ. In each Plaxis simulation, more than one sample can be found for $y(x)$ because it is a x-dependent variable. Database for $y(x)$ will be expanded to $m \times p$ samples where m is number of simulations and p is the number of chosen horizontal locations. Consequently, $y(x)$ can be found by a function with inputs as in Eq. (3), and x as additional input variable:

$$y(x) = f(x, L, EI, H, H_w, B, q, E_{oed}, \gamma_{sat}, \gamma_{unsat}, \phi, c). \quad (3)$$

2.2 Machine learning models

In this section, fundamentals of the chosen ML models, RF and ANN, are discussed. It is noted that attempts on both RF and ANN have been implemented for classification and regression problems. The RFC is chosen for the classification problem of sheet wall safety/failure prediction because of the high accuracy, and stable results. Meanwhile, the ANN models provide a more robust solution for the regression problems compared to that of RF. The model selection process is conventionally applied and not discussed in the study for simplicity.

The cross-validation technique is commonly conducted to observe the randomness of the models, which relies heavily on the accuracy of the data. The conventional method of data splitting into train set, and test set, is a common approach. Further techniques can be applied to capture the dependence of model to data (e.g., K-cross validation [50]). In this study, a set of 1000 RFC models are developed and each of them is developed based on the sampling process of taking 80% of the data from the database [51]. Critical results of the classification problem, which are: accuracy, precision, and recall, for each model on the test set (e.g., the remaining 20% of the database), are calculated. Consequently, the distributions of these metrics are observed to evaluate the dependence of model quality on the database. This process is illustrated in Fig. 2.

2.2.1 The random forest classification

In this paper, the RFC model, predicts the failure status of the sheet wall. The RF method relies on the classification and regression tree algorithm, CART [52], to develop a voting process. Starting with a root node contains the database, CART splits the parent node into the left and the right nodes (or the children nodes) by the best of a pair of t_k and k, where k is the kth feature and t_k is a threshold corresponds to kth feature. The chosen pair of t_k and k must have the minimum following cost function $J(k, t_k)$:

$$J(k, t_k) = \frac{m_{left}}{m} G_{left} + \frac{m_{right}}{m} G_{right}, \quad (4)$$

where $G_{left/right}$ is the impurity of the left/right subset; $m_{left/right}$ is the sample of the left/right subset. The Gini is used in this paper as the impurity measure. With the 2 classes, (0) corresponding to the failure or (1) not failure , the Gini index of a node can be written as:

$$\begin{aligned} G_{left/right} &= 1 - \left(p^2_{left/right|-1} + p^2_{left/right|1}\right) \\ &= 1 - \left(\left(\frac{m_{left/right|-1}}{m_{left/right}}\right)^2 + \left(\frac{m_{left/right|1}}{m_{left/right}}\right)^2\right), \end{aligned} \quad (5)$$

where $p_{left/right|-1}$ is the ratio of instances, belongs to failure class (0) over the total instances in the left/right node. Denominator, $m_{left/right}$ is the number of instances in the left/right node and, $m_{left/right|-1}$ and $m_{left/right|1}$ is the number of instances, belongs to failure and not failure classes, in the left/right node, respectively.

The splitting process is recursively implemented from

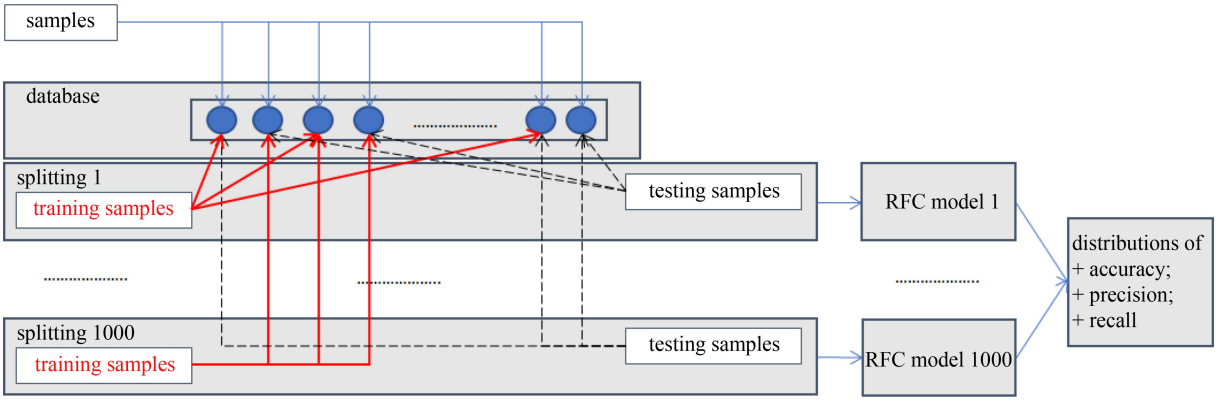

Fig. 2 Illustration of random sampling the data splitting process.

the root node to generate its descendants until the stop condition(s) is reached. The nodes in the last generation are the leaf nodes. In this paper, the main stopping condition are the minimum samples required to split a node, is 2. The minimum samples required to be at a leaf node is 1.

The forest in the RF method, is composed by many CARTs where each of the trees is established based on a part of the FEA database, and n subsets of database are randomly selected from database via boot-strapping (i.e., bagging), or pasting sampling processes, with or without replacement, respectively. The result of the RF is obtained by a voting process, which aggregates the results of all the decision trees. Throughout, the feature importance levels of each input variable, are found based on its influence on establishing the decision trees within a "forest" of trees. To be specific, feature importance level is found from, the average depth in which the feature appeared within the decision trees [53].

2.2.2 The Artificial Neural Network for Regression

The idea of ANN was introduced by McCulloch and Pitts [55] who tried to simulate the mechanics of neurals in the brain. The ANN has a long history of development with various key studies such as image recognition [56], Restricted Boltzmann Machines [57], Deep Belief Net [58], and auto-encoders [59].

A conventional feed-forward ANN is trained by feeding data to the input layer, and each node in this layer takes its corresponding feature of each sample. Every neuron combined its input signals from nodes in the previous layer by weight-summing them. With an activate function (e.g., ReLu, sigmoid or Hyperbolic tangent), this neuron generates a signal to the nodes in the next layer until the output layer is reached. After feeding by so-call batch size b samples, the loss function in Eq. (12) is calculated, and the Back-Propagation algorithm is applied to update the weights of neuron-to-neuron connections.

There are two ANN models, trained separately in this study. The first regression ANN model, RANN1, approximates the lateral displacement of the sheet wall Δ, and the second regression ANN model RANN2, predicts the soil vertical settlement $y(x)$.

2.3 The Proposed Hierarchic System with a Mixture of Classification and Regression models

Once the models successfully developed, a mixture of models is applied as a hierarchic system for designing the process with a logic gate, after the prediction with RFC is conducted (Fig. 3). To avoid the conflict of the final outputs, the conventional binary values of 1 and 0 are used to check the condition. If the sample is labeled as 0 after the RFC, the computing process will stop with the −1 values be assigned for the outputs of RANN1 and RANN2 as the collapse of the sheet wall without actual predictions by these ANN models. Otherwise, if the sample is labeled as 1, the logic gate will trigger the next two regression models, RANN1 and RANN2, to predict lateral displacement at the top of the sheet wall Δ, and the quantity of soil vertical settlement, $y(x)$, respectively. It is noted that the inputs of RANN2 are different from RFC and RANN1 because of the additional x input variables presented for the location along x-axis that are of interest. The output system of the framework in this paper only contains Δ and $y(x)$ and can be developed by adding other outputs of interest such as maximum moment in the sheet wall.

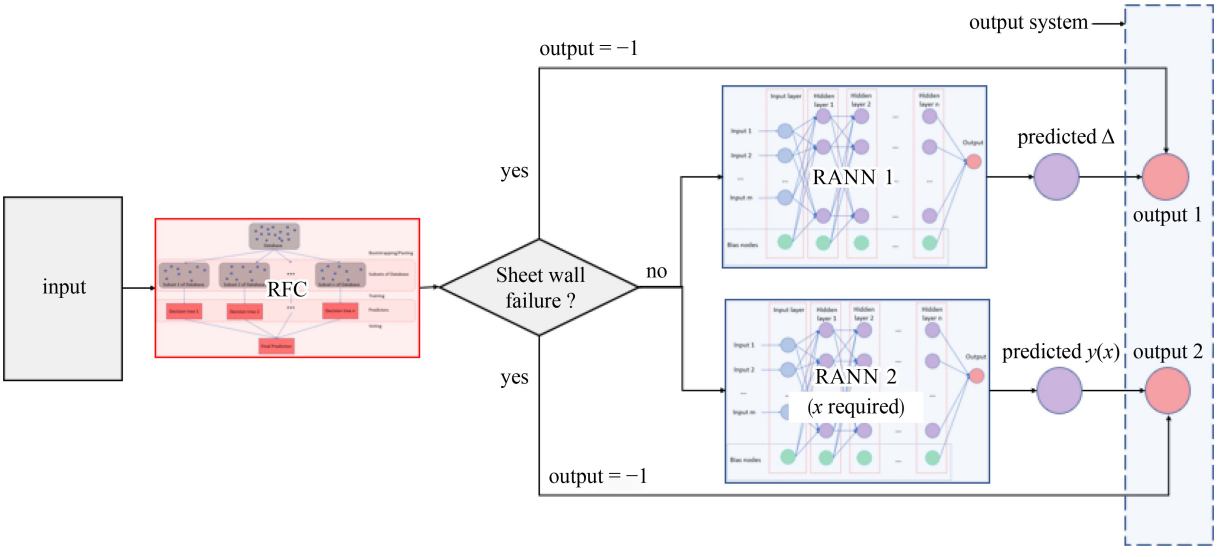

Fig. 3 The proposed system with the mixture of classification and regression and logical gate to find whether a failure occurred.

3 Numerical results

3.1 Validation of hardening soil model and experimental data

A simulation is first conducted with the input variable of the experiment from [60] (listed in Table 1 where H = 5.83 m). The results from Plaxis are provided in a contour plot (Fig. 4). It can be seen in Fig. 4(a) that the maximum disruption of the soil is 100 mm at the bottom of the excavation, and the maximum settlement of the ground is 280 mm near the top of the sheet wall. The adjacent ground surface near the sheet wall (i.e., on the left) settles the most due to the excavation. The more the distance from the top of the sheet wall is, the less the vertical settlement is of the ground surface. In Fig. 4(b), it is reasonable to observe a maximum of the horizontal displacement at the top of the sheet wall is at 380 mm,

Table 1 Inputs of the validating cases (to compare with experimental case) and control case (for parametric study)

No.	variable	unit	validating cases (from Ref. [60])	control case (for parametric study in Subsection 3.4)
1	L	m	10	12
2	EI	kN·m^2/m	6540.7	44982
3	H_w	m	0	2
4	H	m	3.05; 4.05; 5.05; 5.53; 5.83	4
5	q	kN/m^2	0	5
6	B	m	0	5
7	γ_{unsat}	kN/m^3	16	18.0
8	γ_{sat}	kN/m^3	19.85	19.0
9	E_{oed}	kN/m^2	10000	9958
10	c	kN/m^2	0	1
11	phi	°	39.4	27

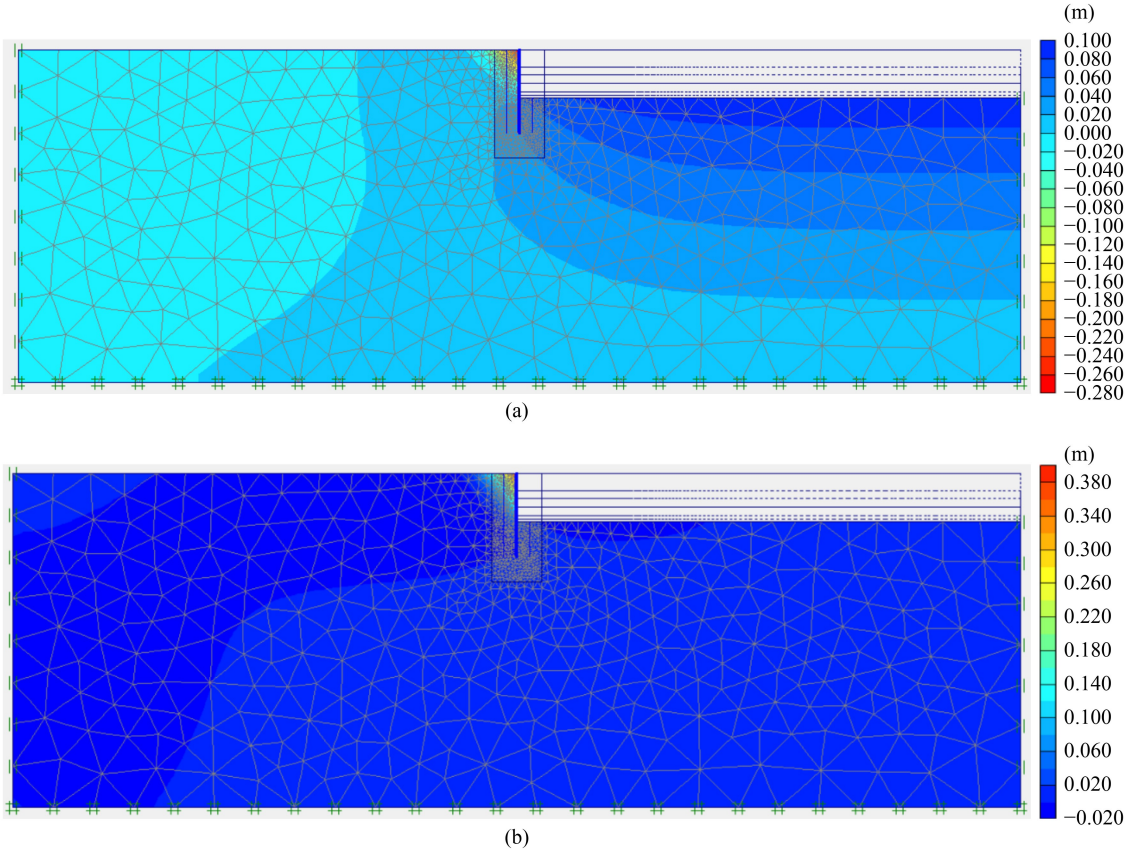

Fig. 4 (a) Vertical displacement and (b) horizontal displacement of soil in the validating case (H = 5.83 m).

and most of points with the significant vertical displacement are concentrated at the back of the wall. In general, results from this observation agree with the intuition on the behaviour of the soil-sheet wall structure.

The results from 5 experiments in Ref. [60] versus the present models are provided in Fig. 5. Despite the existence of differences between the experiment and simulation results, the simulations in these studies provide reasonable values and they closely follow the experimental results. In general, the overall shapes of the corresponding lines are well matched, along with the minor differences between results of simulation and experiment. For instance, differences between displacements at the top of the sheet wall of experiment and simulation are roughly estimated at +20, +10, 15, –25, and –25 mm for the cases of H = 3.05, 4.05, 5.05, 5.53, and 5.83 m, respectively. This comparison validates the hardening soil model applied in this study which is used for data generating process in the next section.

The case with H = 4.05 m in Fig. 6 is further used to investigate the effect of element size to the output of FEA. The available element types provided by Plaxis are observed, including: the very coarse, coarse, the medium, fine and very fine meshing systems. It can also be seen from Fig. 6 that the results of FEA are converged with the fine sized elements with minor difference between the corresponding lines. The meshing system with finest elements almost matches with the experiment data from Ref. [60]. The horizontal displacement at the top of the cantilever sheet wall Δ, of the very fine and the fine mesh type, are 84.767 and 86.625 mm, respectively. The differences between the finest (Δ = 84.767 mm) and the largest element size (Δ = 98.533 mm) are significant, at 16.240% delta. This indicates that the quality of the FE model depends heavily on the meshing system of the element size. Obviously, a trade-off is unavoidable when the computing time for the very coarse mesh is 357 s, and that of very fine mesh is almost double, with 642 s. To maintain quality of the FEA database, the study consistently uses the very fine meshing system for data generation.

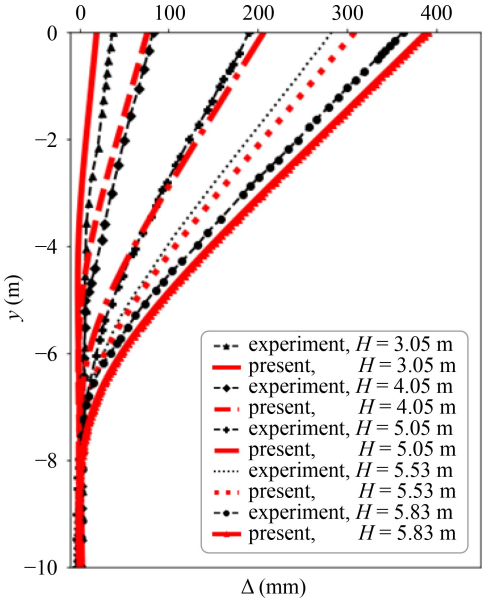

Fig. 5 Horizontal displacements of sheet wall predicted by Hardening Soil simulation in this study versus experiments data from Ref. [60].

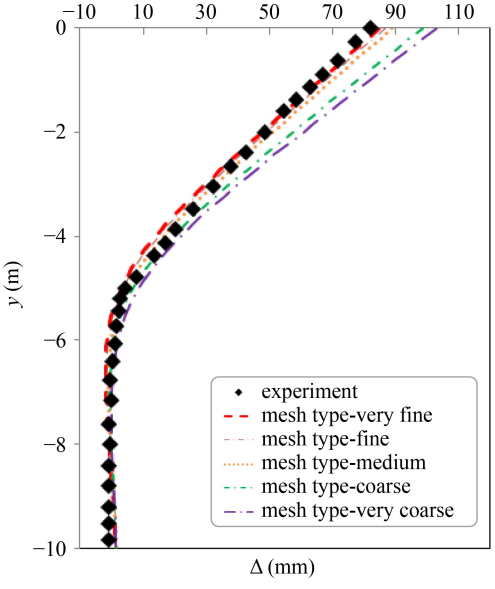

Fig. 6 Comparison of element sizes (experiment data is from Ref. [60]).

3.2 The database and data allocation for training and testing processes

Practically, there is no fixed threshold for the size of the database for an engineering problem, and a sufficient size for database depends on the specific scenarios. In many cases, a few hundred samples in the FEA database are adequate to train a ML model. Examples are, Verma et al. [10] used a database with 100 samples to predict the factor of safety for slopes; 272 data points are used in Ref. [61] to predict settlement of foots; or Duong et al. [16] used a data set of 150 samples to develop ANN model predicting capacity of rectangular concrete-filled steel tube short columns. In this study, the developed database contains the results of 200 FEA samples. It is noted that the database can be expanded if satisfied evaluation metrics of models are not obtained.

A part of the database provided in Tables 2 and 3 and the ranges of the input are in Table 4. These ranges are extremely important for ML prediction because they imply the boundaries of the models. Only if the input variables satisfy such boundaries, the prediction is valid. This is analogous to the extrapolation, if a set of input variables contained value(s) lies outside the

Table 2 Database developed by FEA for stable and Δ

No.	L (m)	EI (kN·m^2/m)	H_w (m)	H (m)	q (kN/m^2)	B (m)	γ_{unsat} (kN/m^3)	γ_{sat} (kN/m^3)	E_{oed} (kN/m^2)	c (kN/m^2)	phi (°)	stable	Δ (mm)	not failure?
1	8	44982	40	5	0	0	18	19	23000	41	15	1	33.61	1
2	9	44982	40	5	0	0	18	19	23000	41	15	1	30.12	1
3	10	44982	40	5	0	0	18	19	23000	41	15	1	28.69	1
4	12	44982	40	5	0	0	18	19	23000	41	15	1	28.14	1
5	16	44982	40	5	0	0	18	19	23000	41	15	1	27.97	1
6	8	44982	40	5	0	0	19	20	9958	1	27	0	–	0*
7	9	44982	40	5	0	0	19	20	9958	1	27	0	–	0*
8	10	44982	40	5	0	0	19	20	9958	1	27	1	211.68	0*
9	12	44982	40	5	0	0	19	20	9958	1	27	1	164.33	1
10	16	44982	40	5	0	0	19	20	9958	1	27	1	155.18	1
⋮	⋮	⋮	⋮	⋮	⋮	⋮	⋮	⋮	⋮	⋮	⋮	⋮	⋮	⋮
198	10	44982	4	5	10	10	19	19.5	12000	32	22	1	40.67	1
199	12	44982	4	5	10	10	19	19.5	12000	32	22	1	39.1	1
200	16	44982	4	5	10	10	19	19.5	12000	32	22	1	39.14	1

*Note: These zero values then switched into –1 in the framework to avoid confusing with the value of regression predictions.

Table 3 Database developed by FEA for $y(x)$

sample #	1		2		…	199		200	
	x (m)	$y(x)$ (m)	x (m)	$y(x)$ (m)	…	x (m)	$y(x)$ (m)	x (m)	$y(x)$ (m)
1	0.0000	0.0082	0.0000	0.0061	…	0.0000	0.0140	0.0000	0.0134
2	0.2951	0.0113	0.2951	0.0092	…	0.2951	0.0232	0.2951	0.0234
3	0.2951	0.0113	0.2951	0.0092	…	0.2951	0.0232	0.2951	0.0234
4	0.6264	0.0123	0.6264	0.0104	…	0.6264	0.0251	0.6264	0.0254
5	0.6264	0.0123	0.6264	0.0104	…	0.6264	0.0251	0.6264	0.0254
⋮	⋮	⋮	⋮	⋮	⋮	⋮	⋮	⋮	⋮
53	55.2219	0.0009	55.2219	0.0009	…	55.2219	0.0019	55.2219	0.0020
54	57.6109	0.0009	57.6109	0.0009	…	57.6109	0.0019	57.6109	0.0019
55	60.0000	0.0009	60.0000	0.0009	…	60.0000	0.0019	60.0000	0.0019

Table 4 Ranges of variables in the database

No.	variable	unit	count	min	max
1	L	(m)	200	8	16
2	EI	(kN·m^2/m)	200	44982	110250
3	H_w	(m)	200	1	40
4	H	(m)	200	2.5	5
5	q	(kN/m^2)	200	0	15
6	B	(m)	200	0	15
7	γ_{unsat}	(kN/m^3)	200	17	19
8	γ_{sat}	(kN/m^3)	200	17.6	20
9	E_{oed}	(kN/m^2)	200	5479	78000
10	c	(kN/m^2)	200	1	41
11	φ	°	200	15	34

corresponding ranges, an inappropriate prediction will occur. Consequently, the developed models are applicable to predict the response of soil-sheet wall with the depth of the excavation is up to 5 m. Other input ranges can be found in Table 4. Figure 7 provides the histogram of the Δ and $y(x)$ of the labeled database.

As in the above discussion, a sample is classified as failure if Plaxis warns an error due to the collapse of computing process or the horizontal displacement at the top of the sheet wall exceeds 200 mm. There are 50 samples that are interrupted during the computation process, and 15 samples exceed the threshold for Δ, leading to the failure and not failure categories, containing 65 and 135 samples, respectively. The ratio number of failure/total number of stable samples is (200–135)/200 = 0.325 indicating an unbalanced database or more samples are in safe condition. The labeled database is first split in to the train set, and test set, with 80% of the database as the train set. This train set (160 samples) is then used for the training process to develop

the model, and the test set (40 samples) is used for validating the model.

To predict Δ, only 135 samples which are labeled as stable category are used to develop the RANN1. This data set is randomly split again into train set (108 samples) and test set (27 samples). Analogous to this of RANN1, data for RANN2 is generated from 135 non-failure samples. For each of these 135 simulations, $y(x)$ at a set of 31 horizontal locations, x is recorded. To validate the effectiveness of developed model, 5 samples are randomly chosen for the final illustration, which are the 1st, 33rd, 96th, 101st, and 140th samples. These 5 samples provide the validation of RANN2 on an unfamiliar data set. The rest of the database (130 simulations) provides 130 × 31 = 4030 samples and then splits into the train and test sets with the ratio of 8:2, respectively. The train set thus contains 104 × 31 = 3224 samples and the test set contains 26 × 31 = 806 samples. Details of the data allocation are provided in Table 5.

Table 6 provides the insight relationships of the input and output variables within the database developed from FEA. It is worthy to note that each row of this table is calculated from different databases corresponding to the data1, data2, and data3 designated in Data ID column Table 5. The Kendall correlation coefficients in Table 6 are slightly low, with many values close to zero and the maximum absolute value is 0.4753 as compared to the maximum at 1.0000 for this factor. However, various papers focusing on ML, have developed quality models with inputs, which have correlation coefficients that are less than 0.5000 such as Ref. [62].

It can be seen from Table 6 that critical inputs for predicting the stable and Δ share similarity to some level. To begin, L, c, and E_{oed}, are the most significant inputs with the values within 0.3 to 0.45. Width of the applied load, B, and saturated weighted, γ_{sat}, are at the medium level to their counterparts with the absolute correlation factors ranges within 0.1 to 0.15. Ground water table, H_w, and depth of excavation, H, have the medium correlation to stable and Δ, respectively. Meanwhile, stiffness of the sheet wall, EI, and friction angle, φ, have almost no correlation to outputs.

On the other hand, the vertical displacement of a point on the surface is strongly correlated to x. The quantity and length of applied load on the surface, q and B, tangent stiffness for primary oedometer loading, E_{oed}, friction angle, φ, saturated weight γ_{sat} and unsaturated weight γ_{unsat}, have the highest correlation to $y(x)$. In contrast to the cases of stable and Δ, the length of sheet wall, L, and depth of excavation, H, have weak correlations to the vertical displacement.

3.3 The developed data-driven models

3.3.1 The random forest classification model

As in the above discussion, the data splitting process is repeated randomly to obtain 1000 RFC models with ratio 0.8/0.2 and the critical hyper-parameters of the models are: no maximum of depth of a decision tree is set, minimum samples per leaf is 1, minimum sample for a split (in the decision tree) is 2, and the number of decision trees is 100. Results of distribution of accuracy, precision, and recall, for these RFC, are provided in Fig. 8. It can be seen that the distribution of these metrics are strongly left

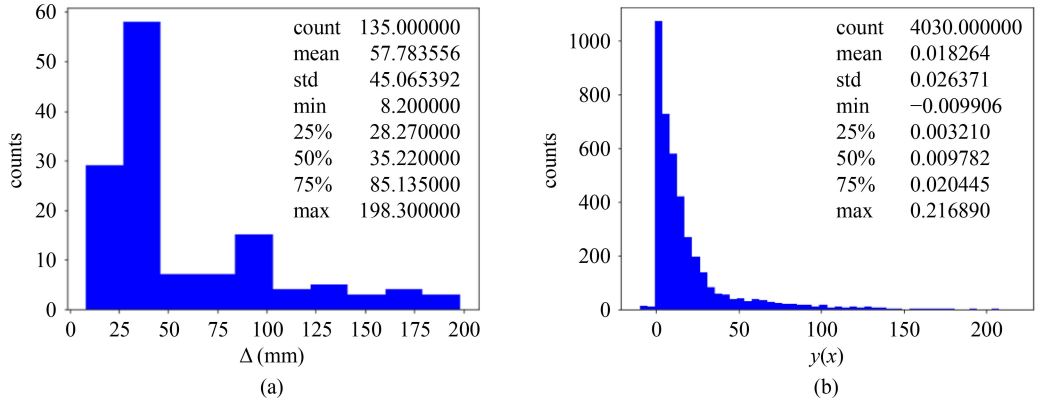

Fig. 7 Histogram of (a) the horizontal displacement of sheet wall and (b) vertical settlement of ground surface.

Table 5 Detail of data splitting for 3 developed models

No.	model	data ID	predicted variable	unit	valid count	min	max	samples for training	samples for testing	samples for graphical evaluation
1	RFC	data1	Status[a)]	–	200	–1	1	160	40	–
2	RANN1	data2	Δ[b)]	mm	135	8.2	200	108	27	–
3	RANN2	data3	$y(x)$[c)]	mm	135 × 31 = 4185[d)]	–13.1	854.7	104 × 31 = 3224	26 × 31 = 806	5[e)] × 31 = 155

Notes: a) Unstable if Δ > 200 mm or error in computation process. b) Only Δ ⩽ 200 mm is used for developing the RANN1. c) Only Δ ⩽ 200 mm is used for developing the RANN2. d) The 31 selected horizontal locations are: 0.0, 0.5, 1.0, 1.5, 2.0, 2.5, 3.0, 3.5, 4.0, 4.5, 5.0, 5.5, 6.0, 6.5, 7.0, 7.5, 8.0, 8.5, 9.0, 9.5, 10.0, 12.0, 14.0, 16.0, 18.0, 20.0, 25.0, 30.0, 40.0, 50.0, 60.0 (m). e) Samples: 1st, 33rd, 96th, 101st, and 140th.

skewed to the natural boundary of 1.0000. Due to this boundary, the median is a better option for expectation observation of these random variables as compared to the mean. It can be seen in Fig. 8 that the recall is significantly lower than its counterparts. This implies the Type I error or false negative is more significant than the Type II error of fault positive for models developed with this database. These lead to the un-conservative side of such models when more actual failure is predicted safety, than actual safety predicted failure. This can be explained by the unbalanced database with more safety samples than failure samples, discussed earlier. For this reason, the recall is the priority evaluation metric in the classification problem, from both practice and database points of view. In the next steps, a model with accuracy, precision, and recall, all equal at 1.0000, is chosen out of the 1000 developed RFC models. The confusion matrix of this chosen model is provided in Fig. 9.

Table 6 Input-output correlation matrix

variable	L	EI	H_w	H	q	B	γ_{unsat}	γ_{sat}	E_{oed}	c	φ	x
stable	0.3674	–0.0642	0.1327	–0.0832	0.1362	0.1184	–0.0698	–0.1439	0.4293	0.4100	–0.0055	–
Δ	0.3235	–0.0447	0.0012	0.1555	–0.1327	–0.1248	0.0838	0.1510	–0.4126	–0.4753	0.0798	–
$y(x)$	0.0614	–0.0077	–0.0771	-0.0374	0.2938	0.2575	–0.2399	–0.2714	–0.3055	–0.3830	0.3683	–0.3926

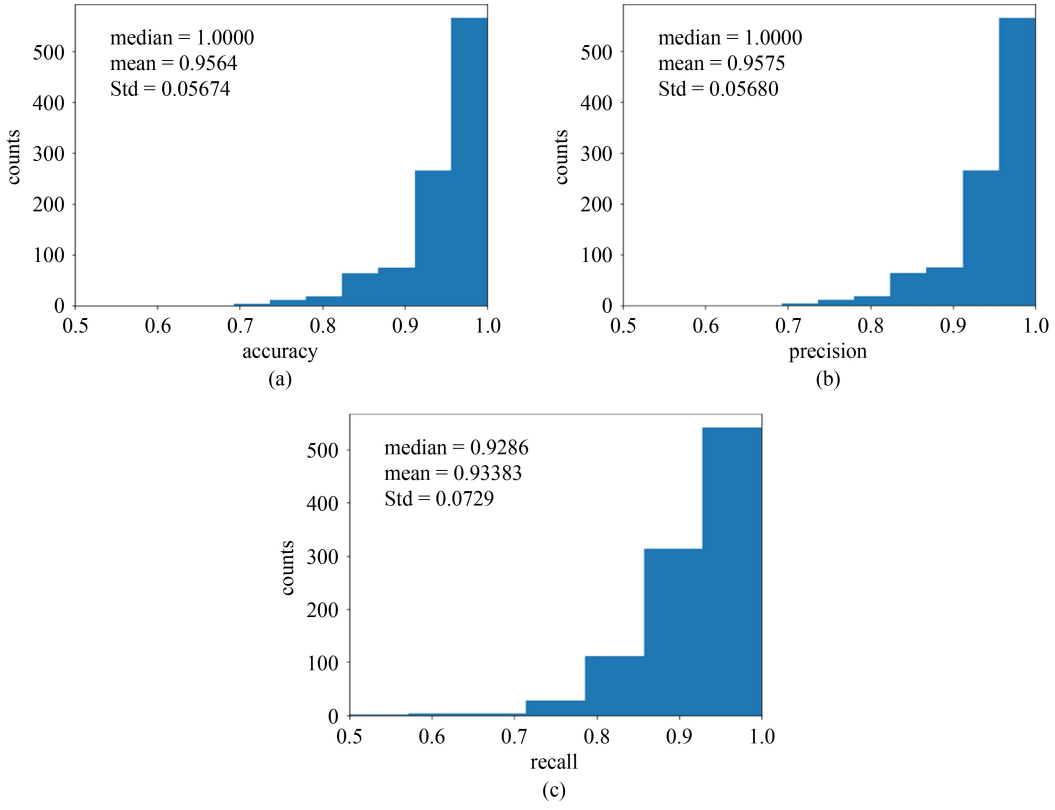

Fig. 8 Evaluation metrics on 1000 RFC based on random splitting database. (a) Accuracy; (b) precision; (c) recall of 1000 RFC models developed from randomly selected sub-databases.

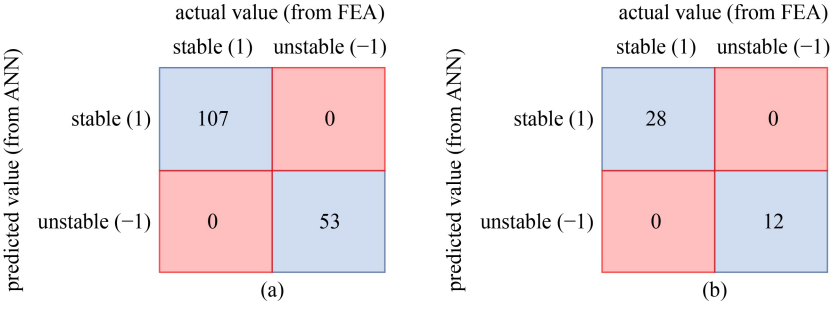

Fig. 9 Confusion matrix of the chosen RFC model on (a) the train data and (b) the test data.

3.3.2 Regression models with artificial neural networks

Since there are no rules to obtain the best network [63], various ANN configurations have been tried with, 10^4 epochs, "adam" optimization algorithm, and Mean Absolute error is the loss function [53]. The batch sizes are 50 and 500 for RANN1 and RANN2, respectively. Details of the chosen configurations for RANN1 and RANN2 are provided in Tables 7 and 8. As can be seen in Table 7, the RANN1 contains 625 nodes, with 3 hidden layers, and 50561 trainable weights. Meanwhile, the RANN2 needs 317 nodes, distributed in 6 hidden layers, with 15729 trainable weights (Table 8).

The evaluation metrics for both RANN1 and RANN2 are provided in Table 9. It can be seen that errors on both test set and train set of RANN1 and RANN2 are all minor compared to the mean values of $y(x)$, and Δ (57.7836 and 18.264, respectively). With a much larger database, it is reasonable to observe that R^2 on test set of RANN2 (0.9988) is much higher than this of RANN1 (0.95212). Figure 10 illustrates the converging process of the ANN models, versus the number of epochs in logarithmic scale. It can be seen from Fig. 10 that the error of RANN1 model (e.g., MAE) on the normalized test set approaches its stable level (MAE is around 0.2000) at 10^3 epochs. Meanwhile, this error value is roughly stable after 2×10^3 epochs in the case of RANN2. Further training for this database may lead to the severe overfitting, when the MAE on the train sets of both models continuously decrease without any improvement of error on the test sets.

It can be seen from Fig. 11, which is a scatter plot of predicted and simulated values of the two models, that the test data points of the two models highly concentrate around 1:1 lines, except a few data points. This is the graphical illustration of the high evaluation metrics of the models in Table 9. Another illustration of the RANN2 is provided in Fig. 12, where the predicted and simulated ground settlement values for sample 1st, 33rd, 96th, 101st, 140th. According to this figure, the RANN2 model successfully predicts ground settlement in both trend, and quantities, despite of some minor errors. The different shapes of the settlement lines are also successfully predicted.

Table 7 Configuration of the RANN1

layer	number of nodes	trainable weights
input layer	12 + 1 (bias)	–
hidden layer 1	64 + 1 (bias)	(12+1) × 64 = 832
hidden layer 2	512 + 1 (bias)	(64+1) × 512 = 33280
hidden layer 3	32 + 1 (bias)	(512+1) × 32 = 16416
output layer	1	(32+1) × 1 = 33
total	625	50561

Table 8 Configuration of the RANN2

layer	number of nodes	trainable weights
input layer	12 + 1(x) + 1 (bias)	–
hidden layer 1	64 + 1 (bias)	(13+1) × 64 = 896
hidden layer 2	64 + 1 (bias)	(64+1) × 64 = 4160
hidden layer 3	64 + 1 (bias)	(64+1) × 64 = 4160
hidden layer 4	64 + 1 (bias)	(64+1) × 64 = 4160
hidden layer 5	32 + 1 (bias)	(64+1) × 32 = 2080
hidden layer 6	8 + 1 (bias)	(32+1) × 8 = 264
output layer	1	(8+1) × 1 = 9
total	317	15729

3.4 Feature importance and parametric studies

To evaluate the impact of inputs to the prediction of RFC model, the feature importance analysis is conducted with normalized results provided in Fig. 13. It can be seen from Fig. 13 that the length of the sheet wall, L, has the critical role with the normalized feature importance score of 0.3186, followed at a distance by E_{oed} (0.1335), and H_w (0.1021). It is reasonable to observe the second ranked position of a variable is related to the soil stiffness, E_{oed}, due to the importance of soil property for maintaining the stability of the retaining wall. Other soil properties (i.e., c, φ, γ_{usat}, γ_{sat}) have low to medium impact to the output with importance factor, ranging from

Table 9 Evaluation metrics for Regression models

metric	equation	RANN1		RANN2	
		on train set	on test set	on train set	on test set
mean absolute error	$MAE = \frac{1}{n} \times \sum_{i=1}^{n} \lvert y_i - f_i \rvert$	0.201697	4.531986	0.000288	0.00103
mean squared error	$MSE = \frac{1}{n} \sum_{i=1}^{n} (y_i - f_i)^2$	0.11290	49.2773	7.2152e−07	9.6209e−06
coefficient of determination	$R^2 = 1 - \frac{\sum_{i=1}^{n} (y_i - f_i)^2}{\sum_{i=1}^{n} (y_i - \bar{y})^2}$	0.9999	0.95212	0.9999	0.9988

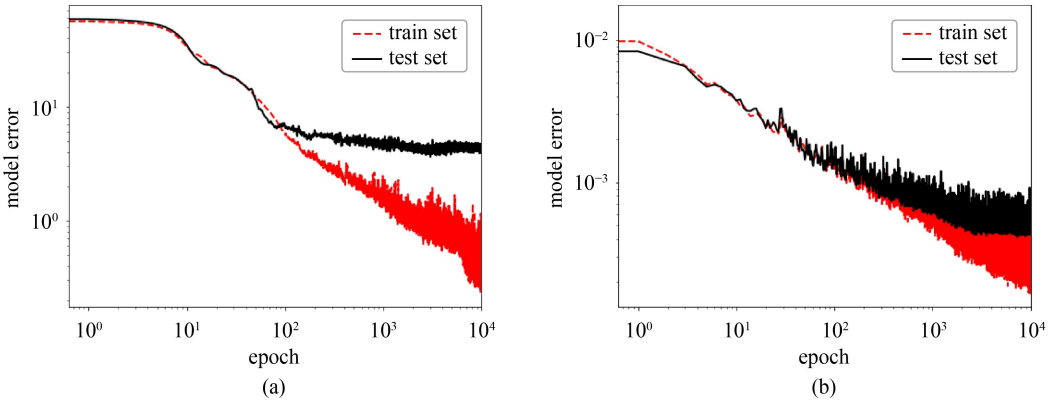

Fig. 10 Model error (MAE) of a) RANN1 and b) RANN2 versus number of epoch (in logarithm scale).

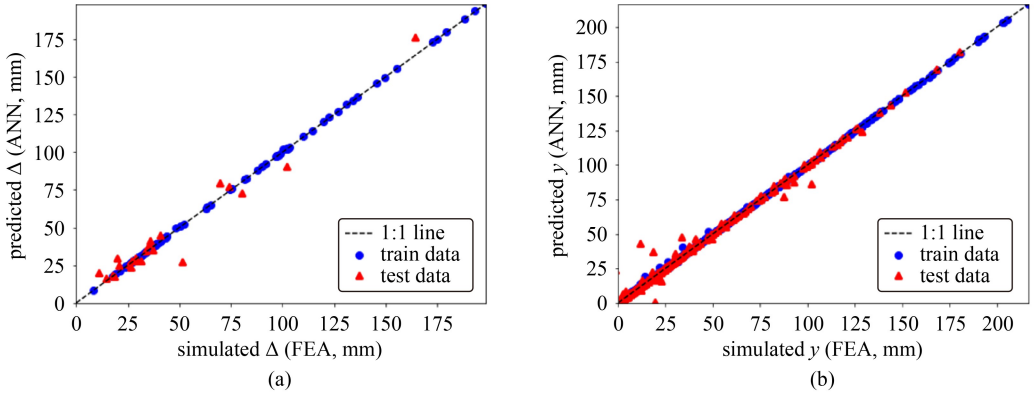

Fig. 11 Predicted values versus simulated values of (a) Δ and (b) $y(x)$.

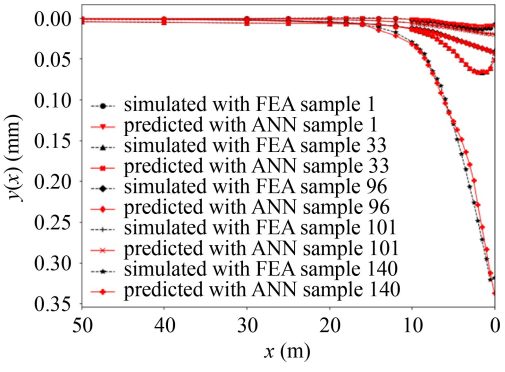

Fig. 12 Graphical illustration predicted versus simulated ground settlement of a set of 5 samples (sample 1st, 33rd, 96th, 101st, 140th).

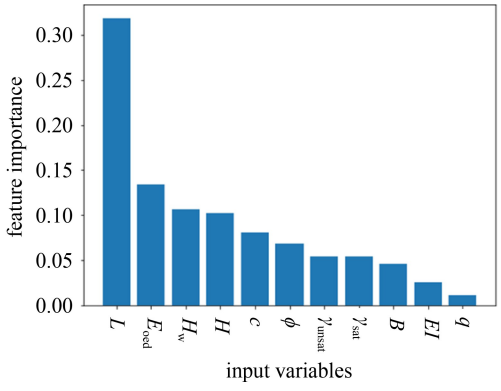

Fig. 13 Feature importance of the RFC model.

0.0834 (c) to 0.0540 (γ_{sat}). Meanwhile, the changes of applied load with corresponding inputs, B and q, and the stiffness of the sheet wall, EI, have minor effect to the prediction, with normalized feature importance levels that are less than 0.0500.

For further observation of inputs to outputs in the developed ML models, the parametric study on RANN1 and RANN2 is implemented. Inputs for the control case for these analyses are given in Table 1. Figures 14 and 15 illustrate the parametric studies for RANN1 and RANN2, respectively.

For RANN1 in Fig.14, the length of sheet wall, L, reinforced its strong effect to the output (i.e., Δ in this scenario) with a clear separation of 8, 10 and 12 m in all sub-figures. For longer walls with L = 14 and 16 m, the differences are minor. In some cases, the corresponding lines of L = 12, 14, and 16 m tend to be overlapped, which implies that the use of these walls has the analogous effects to the system. Figure 16 is intentionally provided with the same scale on y axis with Δ ranging from 0 (mm) to its maximum value of 200 mm. Except for the length of sheet wall, L, the depth of excavation, H, is reasonably having the strongest and positive

correlation, to the displacement of the wall with the exponential lines appeared in the H versus Δ sub-figure. Soil properties have the reversed trends where the increases of E_{oed}, c, γ_{unsat}, and φ, lead to the decrease of Δ. This is predictable because the improvement of soil properties naturally reduce the displacement of the sheet wall. In contrast to the RFC, the changes of ground water table (h_w), width and quantity of applied load (B and q) result in the slight fluctuations of Δ. This implies the less importance of such input variables compared to the

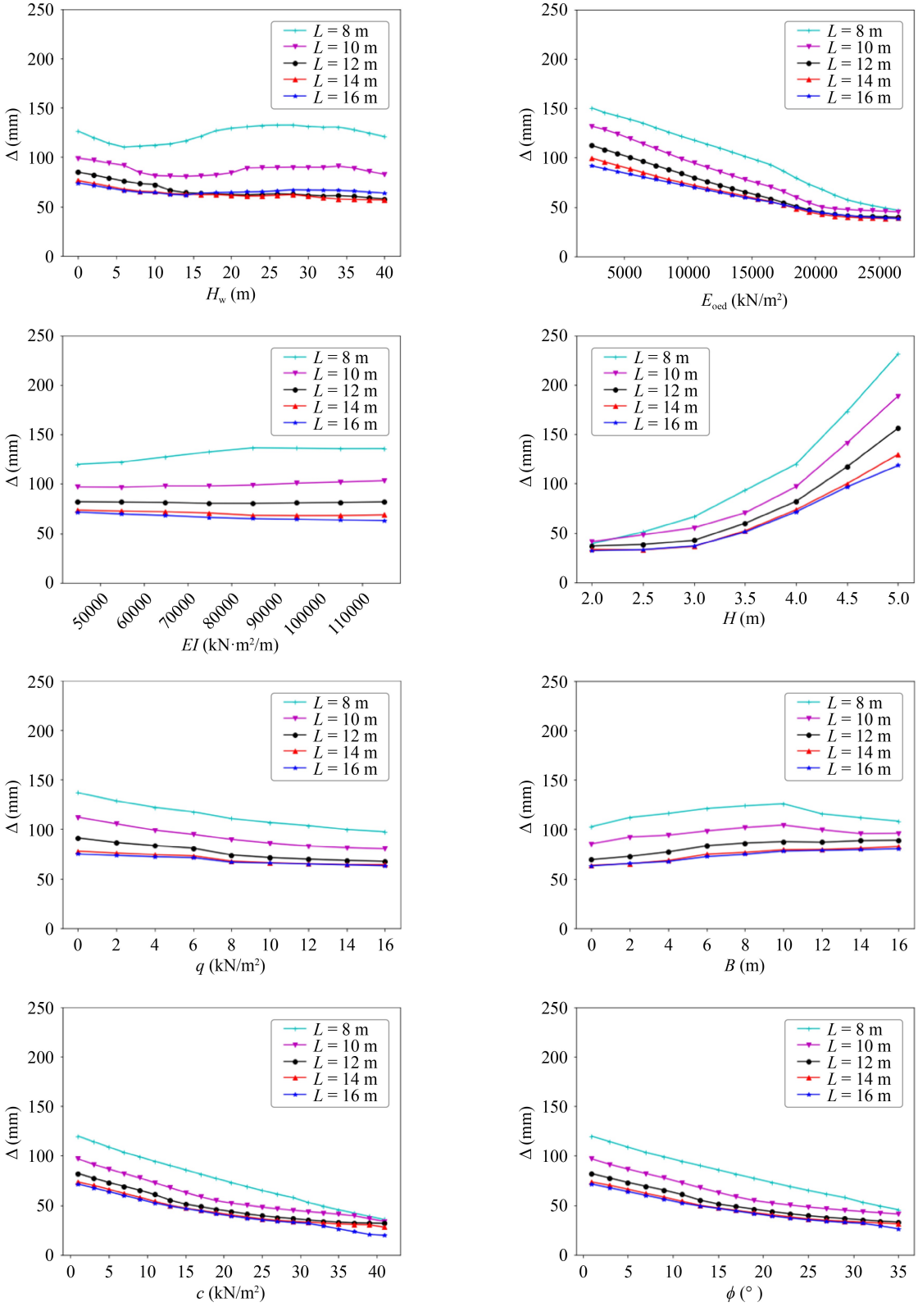

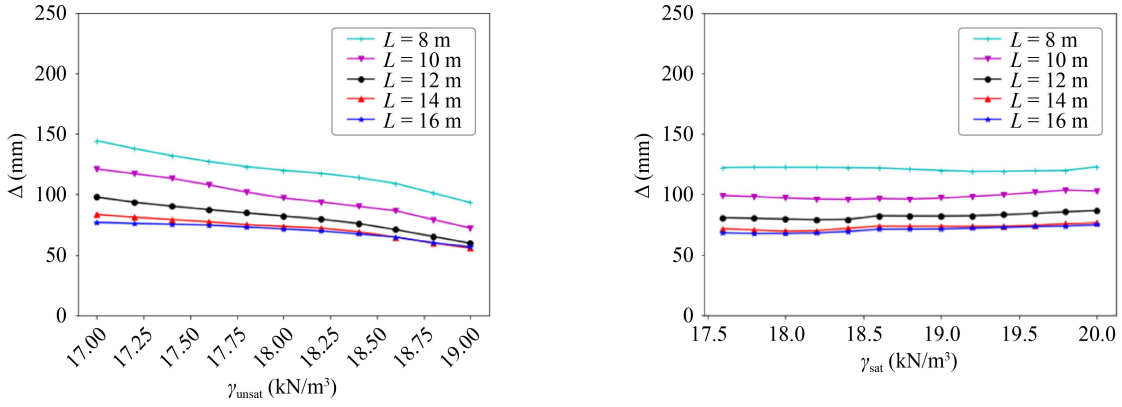

Fig. 14 Parametric study with RANN1.

above-mentioned inputs of RANN1. Sheet wall stiffness, EI, and saturated weight, γ_{sat}, are in the group of features that have the lowest impact to the output.

In Fig.15, results of the parametric study for the RANN2 are provided. The horizontal location of the prediction, x, is the natural key feature of the model with a clear separation of $y(x)$ lines corresponding to the locations adjacent to the sheet wall (e.g., x = 2.5 and 5 m). With further surface points, the differences are minor. This indicates the fading effect of sheet wall existence along with the increase of distance from this structure. The depth of excavation, H, and length of sheet wall, L, and the internal friction angle, φ, are the most critical inputs with dramatic changes of $y(x)$ with the increases of these inputs. While H has the positive correlation with $y(x)$, φ, and L, have the negative effect to the outputs, with the increase of these variables resulting in the decrease of $y(x)$. H_w, c, q, γ_{unsat}, and EI are in the intermediate group which establishes a clear relationship to output. Even though the relationship of E_{oed} and $y(x)$ is apparent, curved-shaped lines are observed with fluctuations. The trends in the B versus $y(x)$ are not clear, with the trends reversed there exists a crossover of x = 2.5 m and x = 5 m lines. The γ_{sat} with the corresponding lines that are almost parallel to the horizontal axis, seems to be the least important variable.

3.5 Results of the proposed hierarchical system

An example is provided of the output system for those proposed in Fig. 3, and the implementation of the 3 developed models, RFC, RANN1 and RANN2, are in

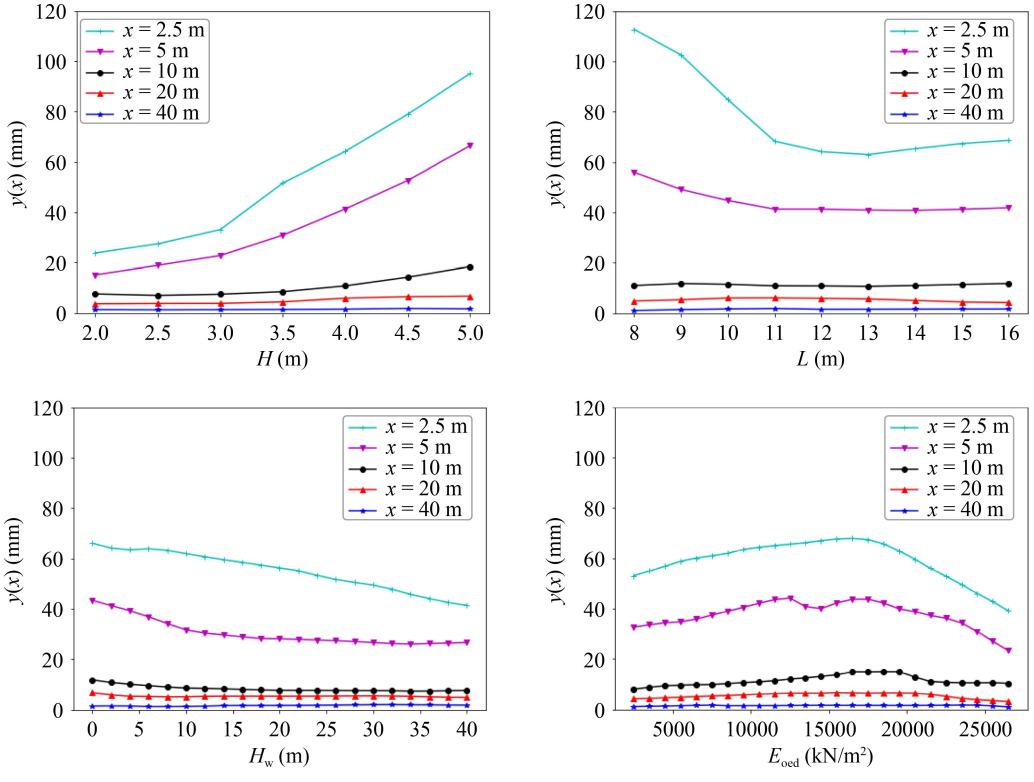

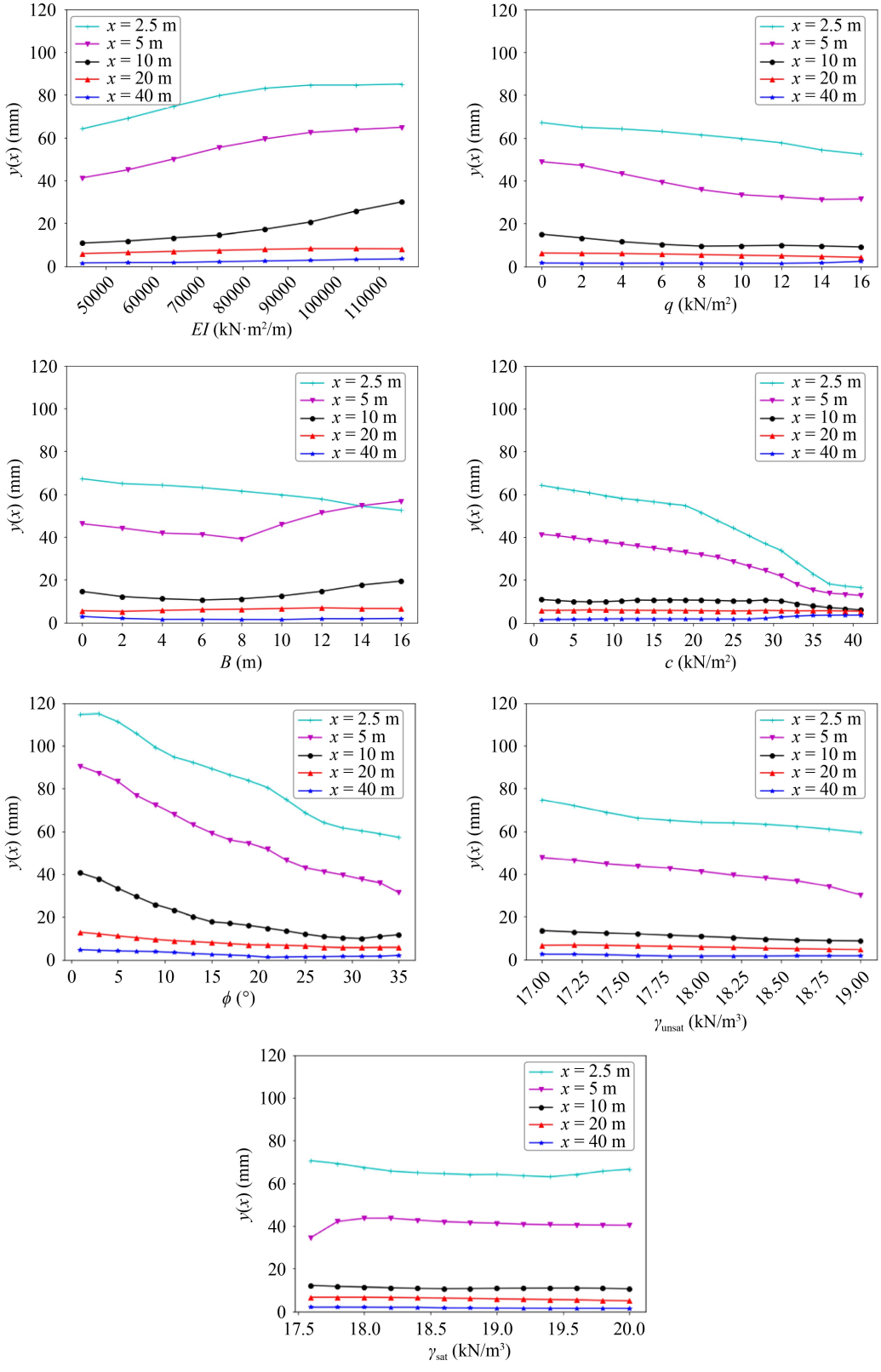

Fig. 15 Parametric study with RANN2.

Table 10 with the comparison from FEA. This output system is not only classifying the failure status of the soil-cantilever sheet wall structure, but also predicting the variables such as Δ and $y(x)$ continuously. For simulation number 1st, 2nd, 3rd, 4th, 5th, 9th, 10th, outputs are positive real values, and imply a not-fail status of these samples. Meanwhile, simulations number 6th, 7th, and 8th are considered as failure. Among those failure cases,

Table 10 Example of output system with proposed framework (Fig. 3)

No.	stable	Δ (FEA) (mm)	x^* (m)	$y(x)$ (FEA) (mm)	not failure?	output 1 (Δ) (mm)	output 2 ($y(x)$) (mm)
1	1	33.610	2.5	12.700	1	30.939	13.200
2	1	30.120	3.5	10.100	1	29.084	98.800
3	1	28.690	4	9.100	1	27.399	9.900
4	1	28.140	0.5	8.700	1	26.209	8.300
5	1	27.970	10	4.400	1	27.932	4.700
6	0	–	–	–	0	–1	–1
7	0	–	–	–	0	–1	–1
8	1	211.680	2.5	22.840	0	–1	–1
9	1	164.330	6.5	29.500	1	149.577	28.900
10	1	155.180	1.5	107.100	1	130.018	112.900

*Note: x location is chosen based on interest. A list of discontinuous x within a range can provide the profile of the settlement on the ground surface.

the 6th and 7th simulations are failed status due to the collapse of soil, and the 8th simulation fails by the exceedance of the condition of $\Delta \leqslant 200$ mm. Even though the $y(x)$ of the 8th simulation is available, it is not provided in the input as a warning of large displacement.

4 Conclusions

In this study, a hierarchical system composed from data-driven models is proposed to predict the behaviour of the soil–cantilever sheet wall structure. In this framework, a classification is conducted to predict the status of soil–sheet wall structure with a trained RF model, RFC. Once the non-failure condition is satisfied, predictions on the variables of interest behaviour of sheet wall and soil, are conducted for the horizontal displacement at the top of the sheet wall Δ with RANN1 model, and the vertical displacement of the surface of the adjacent ground $y(x)$ with RANN2 model.

The use of HS model in Plaxis has been compared with other experiment data before being used as the data generating tool to obtain 200 FEA simulations, and to develop the data-driven models. The classification model has been developed with RF method. The random sampling for the train/test splitting the database has been conducted with 1000 sub-training and 1000 sub-testing sets to develop 1000 RFC models. The distributions of the evaluation metrics of RFC models are observed. To be specific, the medians for accuracy/precision/recall are 1.000/1.000/0.9286; those of means are 0.9564/0.9775/0.9338; and those of standard deviation are 0.05674/0.05680/0.0729, respectively. The negative skewed data toward the absolute value of 1.0000 provides insightful observation of the effect of randomness of the database to the performance of developed models. A RFC model was chosen from the best models of this set of 1000 RFC models, having an accuracy of 1.0 on both train set and test set. With the developed database, RANN1 and RANN2, are the ANN models developed for predicting continuous variables, the Δ, and $y(x)$, respectively. Evaluation metrics of these models on test set are appropriated with low errors and high R^2 (0.9521 for RANN1 and 0.9988 for RANN2).

The analyses on importance level of the inputs for RFC model and parametric studies for ANN models are conducted. The critical inputs for each model are not analogous. Length of the sheet wall, L, E_{oed} and $H_{w,}$ are the most critical inputs for RFC model. Meanwhile, the set of [L and H] and the set of [x, L, H, and φ] are the most important inputs for RANN1 and RANN2, respectively.

To the point, a hierarchical system is proposed and the illustration on how such a system is applied in the engineering problem is provided. It is worth noting that various additions or adjustments may be applied for this system. For example, the check of the Ultimate limit state (model collapse), and the Serviceability limit state ($\Delta \leqslant 200$ mm), can be separated by 2 single models. Other possibilities can be the addition of other interested variables, e.g., maximum moment in the sheet wall. These variations all require an expansion on the database and thus can be improved in future work.

References

1. Kwon J. Investigation of the influence of an excavation on adjacent excavations, using neural networks. Journal of the Southern African Institute of Mining and Metallurgy, 1998, 98(3): 147−156
2. Ramadan M I, Ramadan E H, Khashila M M. Cantilever contiguous pile wall for supporting excavation in clay. Geotechnical and Geological Engineering, 2018, 36(3): 1545−1558
3. Poulos H, Chen L. Pile response due to unsupported excavation-induced lateral soil movement. Canadian Geotechnical Journal, 1996, 33(4): 670−677
4. Bransby P, Milligan G. Soil deformations near cantilever sheet pile walls. Geotechnique, 1975, 25(2): 175−195

5. Singh A P, Chatterjee K. Ground settlement and deflection response of cantilever sheet pile wall subjected to surcharge loading. Indian Geotechnical Journal, 2020, 50(4): 540−549
6. Es-haghi M S, Abbaspour M, Rabczuk T. Factors and failure patterns analysis for undrained seismic bearing capacity of strip footing above void. International Journal of Geomechanics, 2021, 21(10): 04021188
7. Phan H C, Dhar A S. Predicting pipeline burst pressures with machine learning models. International Journal of Pressure Vessels and Piping, 2021, 191: 104384
8. Anitescu C, Atroshchenko E, Alajlan N, Rabczuk T. Artificial neural network methods for the solution of second order boundary value problems. Computers, Materials and Continua, 2019, 59(1): 345−359
9. Samaniego E, Anitescu C, Goswami S, Nguyen-Thanh V M, Guo H, Hamdia K, Zhuang X, Rabczuk T. An energy approach to the solution of partial differential equations in computational mechanics via machine learning: Concepts, implementation and applications. Computer Methods in Applied Mechanics and Engineering, 2020, 362: 112790
10. Verma A K, Singh T N, Chauhan N K, Sarkar K. A hybrid FEM–ANN approach for slope instability prediction. Journal of The Institution of Engineers (India): Series A, 2016, 97(3): 171−180
11. Peng C, Wu W, Zhang B. Three-dimensional simulations of tensile cracks in geomaterials by coupling meshless and finite element method. International Journal for Numerical and Analytical Methods in Geomechanics, 2015, 39(2): 135−154
12. Chakraborty A, Goswami D. Prediction of slope stability using multiple linear regression (MLR) and artificial neural network (ANN). Arabian Journal of Geosciences, 2017, 10(17): 385
13. Chern S, Tsai J H, Chien L K, Huang C Y. Predicting lateral wall deflection in top-down excavation by neural network. International Journal of Offshore and Polar Engineering, 2009, 19(2): 151−157
14. Moayedi H, Mosallanezhad M, Rashid A S A, Jusoh W A W, Muazu M A. A systematic review and meta-analysis of artificial neural network application in geotechnical engineering: Theory and applications. Neural Computing & Applications, 2020, 32(2): 495−518
15. Es-haghi M S, Sarcheshmehpour M. A novel strategy for tall building optimization via combination of asymmetric genetic algorithm and machine learning methods. In: The 1st Online Conference on Algorithms. MDPI, 2021
16. Duong H T, Phan H C, Le T T, Bui N D. Optimization design of rectangular concrete-filled steel tube short columns with Balancing Composite Motion Optimization and data-driven model. Structures, 2020, 28: 757–765
17. Phan H C, Le-Thanh L, Nguyen-Xuan H. A semi-empirical approach and uncertainty analysis to pipes under hydrogen embrittlement degradation. International Journal of Hydrogen Energy, 2022, 47(8): 5677−5691
18. Phan H C, Bui N D. Failure assessment of defected pipe under strike-slip fault with data-driven models accounting to the model uncertainty. Neural Computing & Applications, 2021, 34: 1541−1555
19. Attoh-Okine N, Fekpe E S. Strength characteristics modeling of lateritic soils using adaptive neural networks. Construction & Building Materials, 1996, 10(8): 577−582
20. Pala M, Caglar N, Elmas M, Cevik A, Saribiyik M. Dynamic soil–structure interaction analysis of buildings by neural networks. Construction & Building Materials, 2008, 22(3): 330−342
21. Nazzal M D, Tatari O. Evaluating the use of neural networks and genetic algorithms for prediction of subgrade resilient modulus. International Journal of Pavement Engineering, 2013, 14(4): 364−373
22. Groholski D R, Hashash Y M. Development of an inverse analysis framework for extracting dynamic soil behavior and pore pressure response from downhole array measurements. International Journal for Numerical and Analytical Methods in Geomechanics, 2013, 37(12): 1867−1890
23. Chan W, Chow Y, Liu L. Neural network: An alternative to pile driving formulas. Computers and Geotechnics, 1995, 17(2): 135−156
24. Nazir R, Moayedi H, Pratikso A, Mosallanezhad M. The uplift load capacity of an enlarged base pier embedded in dry sand. Arabian Journal of Geosciences, 2015, 8(9): 7285−7296
25. Ismail A, Jeng D S. Modelling load–settlement behaviour of piles using high-order neural network (HON-PILE model). Engineering Applications of Artificial Intelligence, 2011, 24(5): 813−821
26. Samui P, Sitharam T. Site characterization model using artificial neural network and kriging. International Journal of Geomechanics, 2010, 10(5): 171−180
27. Yilmaz O, Eser M, Berilgen M. Applications of engineering seismology for site characterization. Journal of Earth Science, 2009, 20(3): 546−554
28. Cao Z, Wang Y, Li D. Quantification of prior knowledge in geotechnical site characterization. Engineering Geology, 2016, 203: 107−116
29. Dwivedi V K, Dubey R K, Thockhom S, Pancholi V, Chopra S, Rastogi B K. Assessment of liquefaction potential of soil in Ahmedabad Region, Western India. Journal of Indian Geophysical Union, 2017, 21(2): 116−123
30. Hsein Juang C, Chen C J, Tien Y M. Appraising cone penetration test based liquefaction resistance evaluation methods: Artificial neural network approach. Canadian Geotechnical Journal, 1999, 36(3): 443−454
31. Hanna A M, Ural D, Saygili G. Evaluation of liquefaction potential of soil deposits using artificial neural networks. Engineering Computations, 2007, 24(1): 5−16
32. Liu Z, Shao J, Xu W, Chen H, Zhang Y. An extreme learning machine approach for slope stability evaluation and prediction. Natural Hazards, 2014, 73(2): 787−804
33. Gordan B, Jahed Armaghani D, Hajihassani M, Monjezi M. Prediction of seismic slope stability through combination of particle swarm optimization and neural network. Engineering with Computers, 2016, 32(1): 85−97
34. Li A, Khoo S, Lyamin A V, Wang Y. Rock slope stability analyses using extreme learning neural network and terminal steepest descent algorithm. Automation in Construction, 2016, 65: 42−50
35. Ilia I, Koumantakis I, Rozos D, Koukis G, Tsangaratos P. A geographical information system (GIS) based probabilistic certainty factor approach in assessing landslide susceptibility: The

case study of Kimi, Euboea, Greece. In: IAEG XII Congress: Engineering Geology for Society and Territory. Turin: Springer, 2015: 1199−1204

36. Souza F, Ebecken N. A data mining approach to landslide prediction. WIT Transactions on Information and Communication Technologies, 2004: 33
37. Melchiorre C, Matteucci M, Azzoni A, Zanchi A. Artificial neural networks and cluster analysis in landslide susceptibility zonation. Geomorphology, 2008, 94(3-4): 379−400
38. Huang F K, Wang G S. ANN-based reliability analysis for deep excavation. In: EUROCON 2007—The International Conference on "Computer as a Tool". Warsaw: IEEE, 2007
39. Goh A T, Wong K, Broms B. Estimation of lateral wall movements in braced excavations using neural networks. Canadian Geotechnical Journal, 1995, 32(6): 1059−1064
40. Jan J, Hung S L, Chi S Y, Chern J C. Neural network forecast model in deep excavation. Journal of Computing in Civil Engineering, 2002, 16(1): 59−65
41. Jun Y, Haiming C. Artificial neural network's application in intelligent prediction of surface settlement induced by foundation pit excavation. In: 2009 Second International Conference on Intelligent Computation Technology and Automation. Zhangjiajie: IEEE, 2009
42. Koy C, Yune C Y. Numerical analysis on consolidation of soft clay by sand drain with heat injection. Journal of the Korean Geotechnical Society, 2017, 33(11): 45−57
43. Zhou J, Shi X, Du K, Qiu X, Li X, Mitri H S. Feasibility of random-forest approach for prediction of ground settlements induced by the construction of a shield-driven tunnel. International Journal of Geomechanics, 2017, 17(6): 04016129
44. Nikbakht S, Anitescu C, Rabczuk T. Optimizing the neural network hyperparameters utilizing genetic algorithm. Journal of Zhejiang University, Science A, 2021, 22(6): 407−426
45. Zhang W, Zhang R, Wu C, Goh A T C, Lacasse S, Liu Z, Liu H. State-of-the-art review of soft computing applications in underground excavations. Geoscience Frontiers, 2020, 11(4): 1095−1106
46. Schanz T, Vermeer P A, Bonnier P G. Beyond 2000 in Computational Geotechnics. London: Routledge, 1999: 281−296
47. Ou C Y, Lai C H. Finite-element analysis of deep excavation in layered sandy and clayey soil deposits. Canadian Geotechnical Journal, 1994, 31(2): 204−214
48. Mansour M, Rashed A, Farag A. Adopting numerical models for prediction of ground movements induced by deep excavation. International Journal of Recent Technology and Engineering, 2020, 8(6): 976−988
49. Brinkgreve R B J, Swolfs W M, Engin E, Waterman D, Chesaru A, Bonnier P, Galavi V. PLAXIS 2D Reference Manual. Delft: Delft University of Technology and PLAXIS bv, 2011
50. Le T T, Phan H C. Prediction of ultimate load of rectangular CFST columns using interpretable machine learning method. Advances in Civil Engineering, 2020, 2020: 8855069
51. Le T T. Prediction of tensile strength of polymer carbon nanotube composites using practical machine learning method. Journal of Composite Materials, 2021, 55(6): 787−811
52. Breiman L, Breiman L, Friedman J H, Olshen R A, Stone C J. Classification and Regression Trees. Boca Raton: Chapman & Hall, 1984
53. Géron A. Hands-On Machine Learning with Scikit-Learn, Keras, and TensorFlow: Concepts, Tools, and Techniques to Build Intelligent Systems. Sebastopol: O'Reilly Media, 2019
54. Pham T D, Bui N D, Nguyen T T, Phan H C. Predicting the reduction of embankment pressure on the surface of the soft ground reinforced by sand drain with random forest regression. IOP Conference Series: Materials Science and Engineering, 2020, 869(7): 072027
55. McCulloch W S, Pitts W. A logical calculus of the ideas immanent in nervous activity. Bulletin of Mathematical Biophysics, 1943, 5(4): 115−133
56. LeCun Y, Bengio Y. Convolutional networks for images, speech, and time series. The Handbook of Brain Theory and Neural Networks, 1995, 3361(10): 1−14
57. Carreira-Perpinan M A, Hinton G E. On contrastive divergence learning. In: The Tenth International Workshop on Artificial Intelligence and Statistics. Barbados: PMLR, 2005: 33−40
58. Hinton G E, Osindero S, Teh Y W. A fast learning algorithm for deep belief nets. Neural Computation, 2006, 18(7): 1527−1554
59. Ranzato M A, Huang F J, Boureau Y L, LeCun Y. Unsupervised learning of invariant feature hierarchies with applications to object recognition. In: 2007 IEEE Conference on Computer Vision and Pattern Recognition. Minneapolis: IEEE, 2007
60. Chogueur A, Abdeldjalil Z, Reiffsteck P. Parametric and comparative study of a flexible retaining wall. Periodica Polytechnica. Civil Engineering, 2018, 62(2): 295−307
61. Shahin M A, Jaksa M B, Maier H R. Artificial neural network applications in geotechnical engineering. Australian Geomechanics, 2001, 36(1): 49−62
62. Phan H C, Le T T, Bui N D, Duong H T, Pham T D. An empirical model for bending capacity of defected pipe combined with axial load. International Journal of Pressure Vessels and Piping, 2021, 191: 104368
63. Phan H C, Duong H T. Predicting burst pressure of defected pipeline with principal component analysis and adaptive neuro fuzzy inference system. International Journal of Pressure Vessels and Piping, 2021, 189: 104274